

S_4 Symmetric Microscopic Model for Iron-Based Superconductors

Jiangping Hu^{1,2} and Ningning Hao^{1,2}

¹*Beijing National Laboratory for Condensed Matter Physics, Institute of Physics,
Chinese Academy of Sciences, Beijing 100080, China*

²*Department of Physics, Purdue University, West Lafayette, Indiana 47907, USA*
(Received 8 March 2012; published 30 May 2012)

Although iron-based superconductors are multiorbital systems with complicated band structures, we demonstrate that the low-energy physics which is responsible for their high- T_c superconductivity is essentially governed by an effective two-orbital Hamiltonian near half filling. This underlying electronic structure is protected by the S_4 symmetry. With repulsive or strong next-nearest-neighbor antiferromagnetic exchange interactions, the model results in a robust A_{1g} s -wave pairing which can be mapped exactly to the d -wave pairing observed in cuprates. The classification of the superconducting (SC) states according to the S_4 symmetry leads to a natural prediction of the existence of two different phases, named the A and B phases. In the B phase, the superconducting order has an overall sign change along the c axis between the top and bottom As (or Se) planes in a single Fe-As (or Fe-Se) trilayer structure, the common building block of iron-based superconductors. The sign change is analogous to the sign change in the d -wave superconducting state of cuprates upon 90° rotation. Our derivation provides a unified understanding of iron pnictides and iron chalcogenides, and suggests that cuprates and iron-based superconductors share an identical high- T_c superconducting mechanism.

DOI: [10.1103/PhysRevX.2.021009](https://doi.org/10.1103/PhysRevX.2.021009)

Subject Areas: Condensed Matter Physics, Strongly Correlated Materials, Superconductivity

I. INTRODUCTION

Since the discovery of iron-based superconductors [1–4], there has been considerable controversy over the choice of the appropriate microscopic Hamiltonian [5,6]. The major reason behind such a controversy is the complicated multiple- d -orbital electronic structure of the materials. Although the electronic structure has been modeled by using different numbers of orbitals, ranging from a minimum of two [7], to three orbitals [8], and to all five d orbitals [9,10], a general perception has been that any microscopic model composed of fewer than all five d orbitals and ten bands is insufficient [6]. Such a perception has blocked the path to understanding the superconducting mechanism because of the difficulty in identifying the key physics responsible for the high T_c . Realistically, in a model with five orbitals, it is very difficult for any theoretical calculation to make meaningful predictions in a controllable manner.

Iron-based superconductors include two families: iron pnictides [1–3] and iron chalcogenides [4]. The families share many intriguing common properties. They both have the highest T_c s around 50 K [2,5,11–13]. The superconducting gaps are close to being isotropic around Fermi

surfaces [14–19], and the ratio between the gap and T_c , $2\Delta/T_c$, is much larger than the Bardeen-Cooper-Schrieffer ratio, 3.52, in both families. However, the electronic structures in the two families, in particular, the Fermi surface topologies, are quite different in the materials that reach high T_c . The hole pockets are absent in iron chalcogenides but present in iron pnictides [14,17–19]. The presence of the hole pockets has been necessary for superconductivity in the majority of studies and models which strongly depend on the properties of Fermi surfaces. Therefore, the absence of the hole pockets in iron chalcogenides has led to an intense debate over whether both families belong to the same category and share a common superconducting mechanism. Without a clear microscopic picture of the underlying electronic structure, such a debate cannot be settled.

When they are observed by angle-resolved photoemission microscopy (ARPES), a very intriguing property noted in the SC states of iron pnictides is that the SC gaps on different Fermi surfaces are nearly proportional to a simple form factor $\cos k_x \cos k_y$ in the reciprocal space. This form factor has been observed in two families of iron pnictides: the 122 family (such as $\text{Ba}_{1-x}\text{K}_x\text{Fe}_2\text{As}_2$) [14,15,20,21] and the 111 family (such as $\text{NaFe}_{1-x}\text{Co}_x\text{As}$) [22,23]. Just like the d -wave form factor $(\cos k_x - \cos k_y)$ in cuprates, such a form factor indicates that the pairing between two next-nearest-neighbor iron sites in real space dominates. In contrast, in a multiorbital model, many theoretical

Published by the American Physical Society under the terms of the Creative Commons Attribution 3.0 License. Further distribution of this work must maintain attribution to the author(s) and the published article's title, journal citation, and DOI.

calculations based on weak-coupling approaches have shown that the gap functions are very sensitive to detailed band structures and vary significantly when the doping changes [6,24–28]. The robustness of the form factor has therefore been argued to favor strong-coupling approaches, which emphasize electron-electron correlation or the effective next-nearest-neighbor (NNN) antiferromagnetic (AF) exchange coupling J_2 [29–35] as a primary source of the pairing force. However, realistically, it is very difficult to imagine that such a local exchange interaction remains identical between all d -orbital electrons if a multiple- d -orbital model is considered.

In this paper, we demonstrate that the underlying electronic structure in iron-based superconductors, the low-energy physics responsible for superconductivity, is essentially governed by a two-orbital model obeying the S_4 symmetry. The two-orbital model includes two nearly degenerate single-orbital parts that can be mapped to each other under the S_4 transformation. This electronic structure stems from the fact that the dynamics of the d_{xz} and d_{yz} orbitals are divided into two groups that are separately coupled to the top and bottom As(Se) planes in a single Fe-(As)Se trilayer structure. [Throughout the paper, Fe-(As)Se means either the Fe-As or Fe-Se trilayer structure, the common building block of iron-based superconductors. Similarly, As(Se) means either As or Se.] The two groups can thus be treated as an S_4 isospin. The dressing of other orbitals in the d_{xz} and d_{yz} orbitals cannot alter the characteristics of the symmetry.

The underlying electronic structure becomes transparent after one performs a gauge mapping in the five-orbital model [10]. The gauge mapping also reveals the equivalence between the A_{1g} s -wave pairing and the d -wave pairing. After the gauge mapping, the band structure for each S_4 isospin component is characterized by Fermi surfaces located around the anti- d -wave nodal points in the Brillouin zone, corresponding to the sublattice periodicity of the bipartite iron square lattice, as shown in Fig. 1(a). In the presence of an AF exchange coupling J_2 or an effective on-site Hubbard interaction, the d -wave pairing defined in the sublattices can be argued to be favored, just like the case in cuprates. The d -wave pairing symmetry maps reversely to an A_{1g} s -wave pairing in the original gauge setting. These results provide a unified microscopic understanding of iron pnictides and iron chalcogenides and explain why an s -wave SC state without the sign change on Fermi surfaces in iron chalcogenides driven by repulsive interaction can be so robust. Even more intriguing, since the different gauge settings do not alter any physical measurements, the results suggest that, in the A_{1g} s -wave state, for each S_4 isospin component, there is a hidden sign change between the top As(Se) and the bottom As(Se) planes along the c axis.

The S_4 symmetry adds a new symmetry classification to the SC states. For example, even in the A_{1g} s -wave

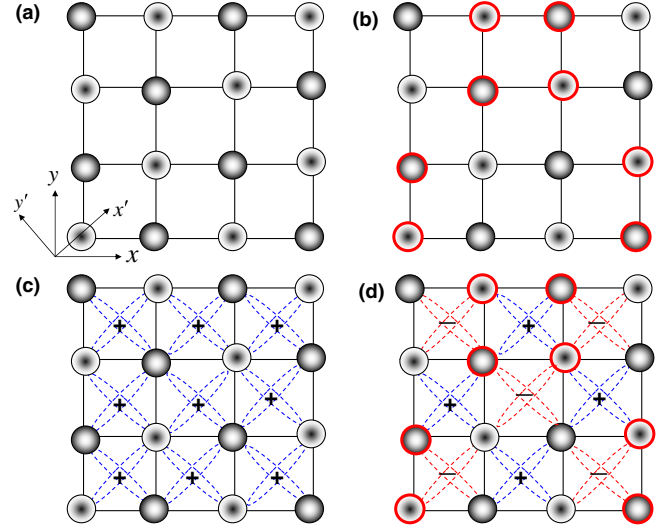


FIG. 1. (a) The square lattice structure of a single iron layer: One cell includes two Fe ions shown as differently filled black balls forming two sublattices. We use x - y coordinates to mark the original tetragonal lattices and x' - y' to mark the sublattice direction. (b) The gauge transformation is illustrated. The balls with red circles are affected by the gauge transformation. (c) and (d) The mapping from the s -wave to the d -wave pairing symmetry by the gauge transformation.

pairing state, there are the two phases, A and B , with respect to the S_4 symmetry. In the A phase, the relative SC phase between the two S_4 isospin components is zero, while, in the B phase, the relative SC phase is π . Therefore, there is an overall π phase shift between the top As(Se) and the bottom As(Se) planes in the B phase along the c axis. Such a sign change should be detectable experimentally. This property makes iron-based superconductors useful in many SC device applications. An experimental setup, similar to those for determining the d -wave pairing in cuprates [36–38], is proposed to detect the π phase shift. The detection of the sign change will strongly support the premise that cuprates and iron-based superconductors share an identical microscopic superconducting mechanism and will establish that repulsive interactions are responsible for superconductivity.

The paper is organized in the following way. In Sec. II, we perform a gauge mapping and discuss the emergence of the underlying electronic structure. In Sec. III, we show that the underlying electronic structure can be constructed by a two-orbital model obeying the S_4 symmetry and discuss many general properties of the model. In Sec. IV, we discuss the classification of the SC states under the S_4 symmetry and propose a measurement to detect the π phase shift along the c axis between the top and bottom As(Se) planes. In Sec. V, we discuss the analogy between iron-based superconductors and cuprates.

II. GAUGE MAPPING AND THE EQUIVALENCE OF s -WAVE AND d -WAVE PAIRING

A. Gauge mapping

We start by asking whether there is an unidentified important electronic structure in iron-based superconductors in a different gauge setting. We give a translationally invariant Hamiltonian that describes the electronic band structure of an Fe square lattice,

$$\hat{H}_0 = \sum_{ij,\alpha\beta,\sigma} t_{ij,\alpha\beta} \hat{f}_{i\alpha,\sigma}^\dagger \hat{f}_{j\beta,\sigma}, \quad (1)$$

where i, j label Fe sites; α, β label orbitals; and σ labels spin. We consider the following gauge transformation. As shown in Figs. 1(a) and 1(b), we group four neighboring iron sites to form a super site, and we mark half of the super sites in red. The gauge transformation, \hat{U} , adds a minus sign to all Fermionic operators $\hat{f}_{i\alpha,\sigma}$ at every site i marked in red. After the transformation, the Hamiltonian becomes

$$\hat{H}'_0 = \hat{U}^\dagger \hat{H}_0 \hat{U}. \quad (2)$$

The gauge-mapping operator \hat{U} is a unitary operator so the eigenvalues of \hat{H}_0 are not changed after the gauge transformation. It is also important to notice that the mapping does not change any standard interaction terms, such as conventional electron-electron interactions and spin-spin exchange couplings. Namely, for a general Hamiltonian including interaction terms \hat{H}_I , under the mapping, we obtain

$$\hat{H} = \hat{H}_0 + \hat{H}_I \rightarrow \hat{H}' = \hat{U}^\dagger \hat{H} \hat{U} = \hat{H}'_0 + \hat{H}_I. \quad (3)$$

It is also easy to see that every unit cell of the lattice in the new gauge setting includes four iron sites. The original translational invariance of an Fe-As(Se) layer has two Fe

sites per unit cell. As we will show in the following section, the doubling of the unit cell matches the true hidden unit cell in the electronic structure when the orbital degree of freedom is considered. This is the fundamental reason why the new gauge reveals the underlying electronic structure.

B. Equivalence of s -wave and d -wave pairing

The gauge mapping has another important property. As shown in Figs. 1(c) and 1(d), this transformation maps the A_{1g} s -wave $\cos(k_x) \cos(k_y)$ pairing symmetry in the original Fe lattice to a familiar d -wave $\cos k'_x - \cos k'_y$ pairing symmetry defined in the two sublattices, where (k_x, k_y) and (k'_x, k'_y) label momentum in Brillouin zones of the original lattice and sublattice, respectively. A similar mapping has been discussed in the study of a two-orbital iron ladder model [35,39] to address the equivalence of s -wave and d -wave pairing symmetry in one dimension.

In an earlier paper [32], one of us and his collaborator suggested a phenomenological necessity for achieving high T_c and selecting pairing symmetries: When the pairing is driven by a local AF exchange coupling, the pairing form factor has to match the Fermi surface topology in the reciprocal space. If this rule is valid and the iron-based superconductors are in the A_{1g} s -wave state, we expect that the Fermi surfaces after the gauge mapping should be located in the d -wave antinodal points in the sublattice Brillouin zone. This is indeed the case, as we will show in the following sections.

C. Band structures after gauge mapping

Various tight-binding models have been proposed to represent the band structure of \hat{H}_0 . In Fig. 2, we plot the band structure of \hat{H}_0 and the corresponding \hat{H}'_0 for two

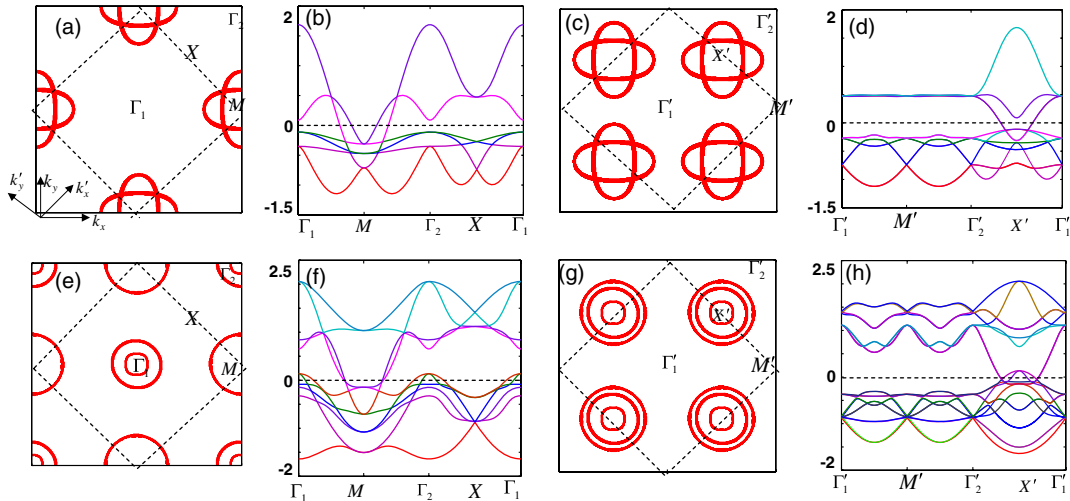


FIG. 2. Three-orbital [30] and five-orbital [10] models: (a),(e) The Fermi surfaces; (b),(f) the band dispersion along the high-symmetry lines; (c),(g) the Fermi surfaces after the gauge transformation; (d),(h) the band dispersions along the high-symmetry lines after the gauge transformation. The hopping parameters can be found in the two references. The y axis for (b),(d),(f),(h) is in units of E(eV).

different models: a maximum five-orbital model for iron pnictides [10], and a three-orbital model constructed for electron-overdoped iron chalcogenides [30].

As shown in Fig. 2, although there are subtle differences among the band structures of H'_0 , striking common features are revealed for both models. First, exactly as expected, all Fermi surfaces after the gauge mapping are relocated around X' , the antinodal points in a standard d -wave superconducting state in the sublattice Brillouin zone. This is remarkable because a robust d -wave superconducting state can be argued to be favored in such a Fermi surface topology in the presence of repulsive interaction or nearest-neighbor (NN) AF coupling in the sublattice [32,40]. If we reversely map to the original gauge, the original Hamiltonian must have a robust s -wave pairing symmetry. Therefore, an equivalence between the A_{1g} s -wave pairing and the d -wave pairing is clearly established by the gauge mapping.

Second, the bands previously located at different places on the Fermi surface are magically linked in the new gauge setting. In particular, the two bands that contribute to electron pockets are nearly degenerate and in the five-orbital model, the bands that contribute to hole pockets are, remarkably, connected to them. Together with the fact that the unit cell has four iron sites in the new gauge setting, these unexpected connections lead us to believe that, in the original gauge, there should be just two orbitals that form bands that make connections from lower-energy bands to higher-energy ones and determine Fermi surfaces. Moreover, the two orbitals should form two groups which provide two nearly degenerate band structures. Finally, since the mapping does not change electron density, Fig. 2 reveals that the doping level in each structure should be close to half filling.

In summary, the gauge mapping reveals that the low-energy physics is controlled by a two-orbital model that produces two nearly degenerate bands.

III. THE CONSTRUCTION OF A TWO-ORBITAL MODEL WITH THE S_4 SYMMETRY

Having made the above observations, we move to construct an effective two-orbital model to capture the underlying electronic structure revealed by the gauge mapping.

A. Physical picture

Our construction is guided by the following several facts. First, the d orbitals that form the bands near the Fermi surfaces are strongly hybridized with the p orbitals of As(Se). Since the $d_{x'z}$ and $d_{y'z}$ have the largest overlap with the $p_{x'}$ and $p_{y'}$ orbitals, it is natural for us to use $d_{x'z}$ and $d_{y'z}$ to construct the model. Second, in the previous construction of a two-orbital model, the C_{4v} symmetry was used [7]. The C_{4v} symmetry is not a correct symmetry, however, if the hopping parameters are generated through

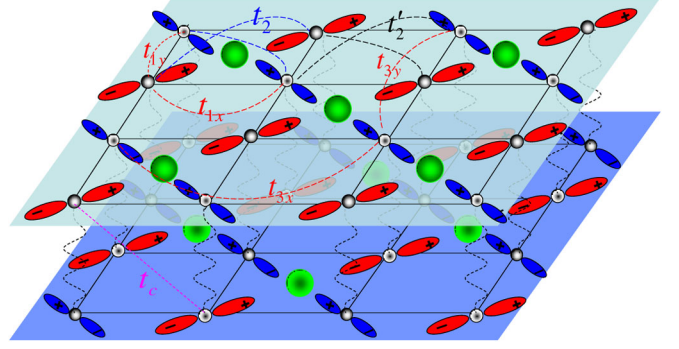


FIG. 3. A sketch of the $d_{x'z}$ and $d_{y'z}$ orbitals, their orientations, and their coupling into the two As(Se) layers. The hopping parameters are indicated: The nearest-neighbor hopping is marked by t_{1x} and t_{1y} ; the next-nearest-neighbor hoppings are t_2 and t'_2 due to the broken symmetry along two different diagonal directions; and the third NN hopping is marked by t_{3x} and t_{3y} . The coupling between the two layers is marked by the nearest-neighbor hopping t_c .

the p orbitals of As(Se). Considering the As(Se) environment, a correct symmetry for the d orbitals at the iron sites is the S_4 symmetry group. Third, there are two As(Se) planes which are separated in space along the c axis. Since there is little coupling between the p orbitals of the two planes, and the hoppings through the p orbitals are expected to dominate over the direct exchange hoppings between the d orbitals themselves, the two-orbital model could essentially be decoupled into two nearly degenerate one-orbital models. Last, the model should have a translational invariance with respect to the As(Se) plane.

Given the above guidelines, it is very natural for us to divide the two d orbitals into two groups, as shown in Fig. 3. One group includes the $d_{x'z}$ in the A sublattice and the $d_{y'z}$ in the B sublattice, and the other includes the $d_{x'z}$ in the B sublattice and the $d_{y'z}$ in the A sublattice, where A and B label the two sublattices of the iron square lattice, as shown in Fig. 1(a). The first group strongly couples to the p orbitals in the upper As(Se) layer, and the second group couples to those in the bottom As(Se) layer. We denote $\hat{c}_{i\sigma}$ and $\hat{d}_{i\sigma}$ as Fermionic operators for the two groups, respectively, at each iron site.

B. S_4 symmetry and the two-orbital model

Without turning on couplings between the two groups, we seek a general tight-binding model to describe the band structure based on the S_4 symmetry. The S_4 transformation maps $\hat{c}_{i\sigma}$ to $\hat{d}_{i\sigma}$. If we define the corresponding operators in the momentum space as $\hat{c}_{k\sigma}$ and $\hat{d}_{k\sigma}$, the S_4 transformation takes

$$\begin{pmatrix} \hat{c}_{k\sigma} \\ \hat{d}_{k\sigma} \end{pmatrix} \rightarrow \begin{pmatrix} -\hat{d}_{k'+Q\sigma} \\ \hat{c}_{k'+Q\sigma} \end{pmatrix}, \quad (4)$$

where $k' = (k_y, -k_x)$ and $Q = (\pi, \pi)$ for given $k = (k_x, k_y)$.

Now, we consider a tight-binding model for the first group. Here we limit the hopping parameters up to the third NN (TNN). As illustrated in Fig. 3, the tight-binding model can be approximated by including NN hoppings (t_{1x} , t_{1y}), NNN hoppings (t_2 , t'_2), and TNN hoppings (t_{3x} , t_{3y}). The longer-range hoppings can be included if needed. For convenience, we can define $t_{1s} = (t_{1x} + t_{1y})/2$, $t_{1d} = (t_{1x} - t_{1y})/2$, $t_{2s} = (t_2 + t'_2)/2$ and

$t_{2d} = (t_2 - t'_2)/2$, $t_{3s} = (t_{3x} + t_{3y})/2$, and $t_{3d} = (t_{3x} - t_{3y})/2$, where the labels s and d indicate hoppings of the s -wave type (where the hopping parameter is symmetric under the 90°-degree rotation) and d -wave type (where the hopping parameter changes sign under the 90°-degree rotation), respectively. A general tight-binding model can be written as

$$\hat{H}_{0,\text{one}} = \sum_{k,\sigma} 2[t_{1s}(\cos k_x + \cos k_y) - \frac{\mu}{2} + t_{1d}(\cos k_x - \cos k_y)]\hat{c}_{k\sigma}^+\hat{c}_{k\sigma} + 4[t_{2s}\cos k_x\cos k_y\hat{c}_{k\sigma}^+\hat{c}_{k\sigma} + t_{2d}\sin k_x\sin k_y\hat{c}_{k\sigma}^+\hat{c}_{k+Q\sigma}] + 2[t_{3s}(\cos 2k_x + \cos 2k_y) + t_{3d}(\cos 2k_x - \cos 2k_y)]\hat{c}_{k\sigma}^+\hat{c}_{k\sigma} + \dots \quad (5)$$

We can apply the S_4 transformation to $\hat{H}_{0,\text{one}}$ to obtain the tight-binding model for the second group. The transformation invariance requires t_{1s} , t_{2d} , and t_{3d} to change signs. Therefore, the two-orbital model is described by

$$\hat{H}_{0,\text{two}} = \sum_{k\sigma} [4t_{2s}\cos k_x\cos k_y - \mu](\hat{c}_{k\sigma}^+\hat{c}_{k\sigma} + \hat{d}_{k\sigma}^+\hat{d}_{k\sigma}) + 2t_{1s}(\cos k_x + \cos k_y)(\hat{c}_{k\sigma}^+\hat{c}_{k\sigma} - \hat{d}_{k\sigma}^+\hat{d}_{k\sigma}) + 2t_{1d}(\cos k_x - \cos k_y)(\hat{c}_{k\sigma}^+\hat{c}_{k\sigma} + \hat{d}_{k\sigma}^+\hat{d}_{k\sigma}) + 4t_{2d}\sin k_x\sin k_y(\hat{c}_{k\sigma}^+\hat{c}_{k+Q\sigma} - \hat{d}_{k\sigma}^+\hat{d}_{k+Q\sigma}) + 2t_{3s}(\cos 2k_x + \cos 2k_y)(\hat{c}_{k\sigma}^+\hat{c}_{k\sigma} + \hat{d}_{k\sigma}^+\hat{d}_{k\sigma}) + 2t_{3d}(\cos 2k_x - \cos 2k_y)(\hat{c}_{k\sigma}^+\hat{c}_{k\sigma} - \hat{d}_{k\sigma}^+\hat{d}_{k\sigma}) + \dots \quad (6)$$

Now we can turn on the couplings between the two groups. It is straightforward to show that the leading order of the couplings that satisfies the S_4 symmetry is given by

$$\hat{H}_{0,c} = \sum_k 2t_c(\cos k_x + \cos k_y)(\hat{c}_{k\sigma}^+\hat{d}_{k\sigma} + \text{H.c.}) \quad (7)$$

Combining $\hat{H}_{0,\text{two}}$ and $\hat{H}_{0,c}$, we obtain an effective S_4 -symmetric two-orbital model whose band structure is described by

$$\hat{H}_{0,\text{eff}} = \hat{H}_{0,\text{two}} + \hat{H}_{0,c} \quad (8)$$

The \hat{c} and \hat{d} Fermionic operators can be viewed as two isospin components of the S_4 symmetry.

Let us assume t_c to be small and check whether $\hat{H}_{0,\text{eff}}$ can capture the electronic structure at low energy. Ignoring t_c , $\hat{H}_{0,\text{eff}}$ provides the following energy dispersions for the two orbitals:

$$E_{e\pm} = \epsilon_k \pm 2t_{3d}(\cos 2k_x - \cos 2k_y) + 4\sqrt{t_{2d}^2\sin^2 x\sin^2 y + \left[\frac{t_{1s}(\cos k_x + \cos k_y) \pm t_{1d}(\cos k_x - \cos k_y)}{2}\right]^2}, \quad (9)$$

$$E_{h\pm} = \epsilon_k \pm 2t_{3d}(\cos 2k_x - \cos 2k_y) - 4\sqrt{t_{2d}^2\sin^2 x\sin^2 y + \left[\frac{t_{1s}(\cos k_x + \cos k_y) \pm t_{1d}(\cos k_x - \cos k_y)}{2}\right]^2}, \quad (10)$$

where $\epsilon_k = 4t_{2s}\cos k_x\cos k_y + 2t_{3s}(\cos 2k_x + \cos 2k_y) - \mu$.

We find that $E_{e\pm}$ can capture the electron pockets at M points and that $E_{h\pm}$ can capture the hole pockets at Γ points. Based on the previous physical picture, t_{1s} , t_{2s} , and t_{2d} should be the largest parameters because they are generated through the p orbitals. In Fig. 4, we show that, by just keeping these three parameters, the model is already good enough to capture the main characteristics of the bands contributing to Fermi surfaces in the five-orbital model. After one performs the same gauge mapping, this Hamiltonian, as expected, provides pockets located at X' , as shown in Fig. 4.

C. General properties of the model

The above model is capable of quantitatively describing the experimental results measured by ARPES [14,20,41–44]. Although the hopping parameters are dominated by t_{1s} , t_{2d} , and t_{2s} , other parameters cannot be ignored. For example, at the same M points, there is energy splitting between two components, which indicates the existence of a sizable t_{1d} . To match the detailed dispersion of the bands, the TNN hoppings have to be included. The existence of the TNN hoppings may also provide a microscopic justification for the presence of the significant TNN AF exchange

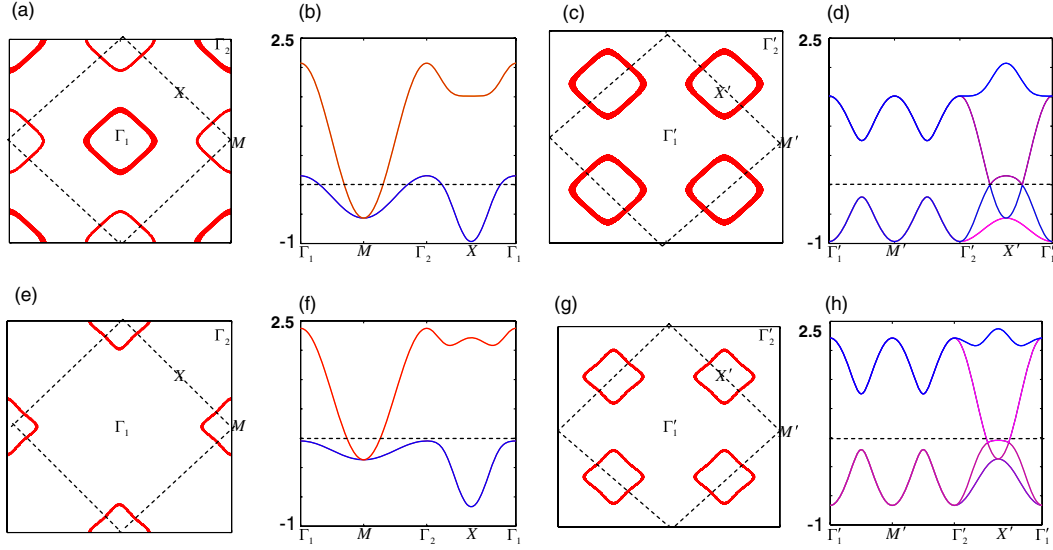


FIG. 4. The Fermi surfaces of each component when only parameters t_{1s} , t_{2d} , and t_{2s} are considered. The layout for (a)–(h) exactly follows that of Fig. 2. The parameters are $t_1 = 0.24$, $t_2 = 0.52$, and $\mu = -0.273$. The only difference in parameters between (a) and (e) is that $t'_2 = -0.1$ in (a) and $t'_2 = -0.2$ in (e). The y axis for (b),(d),(f),(h) is in units of E(ev).

coupling J_3 , measured by neutron scattering in iron chalcogenides [32,45,46].

While the detailed quantitative results for different families of iron-based superconductors will be presented elsewhere [41], we now plot a typical case for iron pnictides with parameters $t_{1s} = 0.4$, $t_{1d} = -0.03$, $t_{2s} = 0.3$, $t_{2d} = 0.6$, $t_{3s} = 0.05$, $t_{3d} = -0.05$, and $\mu = -0.3$ in Figs. 5(a)–5(d). In Figs. 5(a) and 5(b), the coupling $t_c = 0$. In Figs. 5(c) and 5(d), $t_c = 0.02$. It is clear that the degeneracy at the hole pockets along the Γ -X direction is lifted by t_c . The Fermi

surfaces in Fig. 5 are very close to those in the five-orbital model [10]. This result is consistent with our assumption that t_c is effectively small.

The model has several interesting properties. First, it unifies the iron pnictides and iron chalcogenides. When other parameters are fixed, reducing t_{2s} or increasing t_{1s} can flatten the dispersion along the Γ -M direction of $E_{h\pm}$ and cause the hole pocket to vanish completely. Therefore, the model can describe both iron pnictides and electron-overdoped iron chalcogenides by varying t_{2s} or t_{1s} .

Second, carefully examining the hopping parameters, we also find that the NNN hopping for each S_4 isospin essentially has a d -wave symmetry, namely, $|t_{2d}| > t_{2s}$. Since the hole pockets can be suppressed by reducing the value of t_{2s} , this d -wave hopping symmetry is expected to be stronger in iron chalcogenides than in iron pnictides.

Third, it is interesting to point out that we can make an exact analogy between the S_4 transformation on its two isospin components and the time-reversal symmetry transformation on a real 1/2-spin because $S_4^2 = -1$. This analogy suggests that, in this S_4 -symmetric model, the degeneracy at high-symmetry points in the Brillouin zone is of the Kramers type.

Finally, in this model, if the orbital degree of freedom is included, the true unit cell for each isospin component includes four iron atoms. The gauge mapping in the previous section takes exactly a unit cell with four iron sites. Such a match is the essential reason why the low-energy physics becomes transparent after the gauge mapping.

D. The two-orbital model with interactions

By projecting all interactions into these two effective orbital models, a general effective model that describes

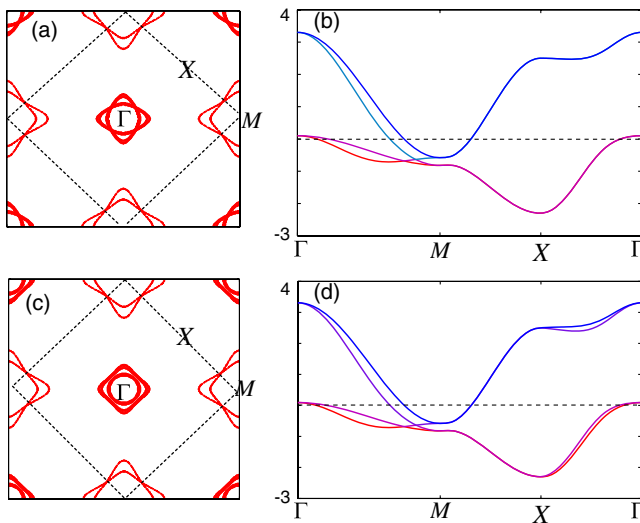


FIG. 5. Typical Fermi surfaces (a) and band dispersions (b) resulting from Eq. (10), with $t_c = 0$ and parameters $t_{1s} = 0.4$, $t_{1d} = -0.03$, $t_{2s} = 0.3$, $t_{2d} = 0.6$, $t_{3s} = 0.05$, $t_{3d} = -0.05$, and $\mu = -0.3$. (c),(d) show the corresponding results when $t_c = 0.02$ is used in Eq. (7) with the same parameter settings. The y axis for (b),(d) is in units of E(ev).

iron-based superconductors obeying the S_4 symmetry can be written as

$$\hat{H}_{\text{eff}} = \hat{H}_{0,\text{eff}} + U \sum_{i,\alpha=1,2} \hat{n}_{i,\alpha} \hat{n}_{i,\alpha} + U' \sum_i \hat{n}_{i,1} \hat{n}_{i,2} + J'_H \sum_i \hat{S}_{i,1} \cdot \hat{S}_{i,2}, \quad (11)$$

where $\alpha = 1, 2$ labels the S_4 isospin, U describes the effective Hubbard repulsion interaction within each component, U' describes the one between them, and J'_H describes the effective Hund's coupling. Since the two components couple weakly, we may expect that U dominates over U' and J'_H . Then, in the first-order approximation, the model could become a single-band Hubbard model near half filling. A similar t - J model can also be discussed within the same context as cuprates [47,48]. It is clear that the model naturally provides an explanation for the stable NNN AF exchange couplings J_2 observed by neutron scattering [45,46,49] and the dominating role of J_2 in both magnetism and superconductivity [32].

E. Reduction of the symmetry from D_{2d} to S_4

The true lattice symmetry in an Fe-As(Se) trilayer is the D_{2d} point group, where S_4 is a subgroup of the D_{2d} . In the D_{2d} group, besides the S_4 invariance, the reflection operator σ_v with respect to the x' - z plane is also invariant. The reflection imposes an additional requirement,

$$\begin{pmatrix} \hat{c}_{k\sigma} \\ \hat{d}_{k\sigma} \end{pmatrix} \rightarrow \begin{pmatrix} \hat{c}_{k''+Q\sigma} \\ -\hat{d}_{k''+Q\sigma} \end{pmatrix}, \quad (12)$$

where $k'' = (k_y, k_x)$. It is easy to see that if we impose the D_{2d} symmetry, the reflection σ_v invariance requires $t_{1s} = 0$. However, without such a reflection invariance, t_{1s} is allowed, which is the case when only the S_4 symmetry remains.

The existence of t_{1s} suggests that σ_v symmetry must be broken in an effective model. However, since σ_v symmetry appears to be present, it is natural to ask what mechanism can break σ_v . While a detailed study of this symmetry breaking is in preparation [50], we give a brief analysis. Among the five d orbitals, d_{xy} , $d_{x^2-y^2}$, and d_{z^2} belong to one-dimensional representations of the D_{2d} group. In fact, for these three orbitals, the D_{2d} group is equivalent to the C_{4v} group. In other words, the As(Se) separation along the c axis has no effect on the symmetry of the kinematics of the three orbitals if the couplings to the other two orbitals, d_{xz} and d_{yz} , are not included. Therefore, for these three orbitals, the unit cell is not doubled by As(Se) atoms, and the band structure is intrinsically one iron per unit cell even if the hoppings generated through p orbitals of As(Se) are important. However, for the d_{xz} and d_{yz} orbitals, if the hoppings through p orbitals of As(Se) are dominant, the unit cell is doubled by As(Se) atoms and the band structure is intrinsically folded. From Eq. (12), after the

S_4 symmetry is maintained, the σ_v -symmetry operations simply map the reduced Brillouin zone to the folded part in the original Brillouin zone. If the couplings between the above two groups of orbitals are turned on, the effective two orbitals that describe the low-energy physics near Fermi surfaces are not pure d_{xz} , d_{yz} orbitals any more. In particular, they are heavily dressed by d_{xy} orbitals, as shown in ARPES [51–54]. Therefore, the effective two orbitals can keep only the S_4 symmetry, and the σ_v symmetry has to be broken.

Another possibility for generation of the t_{1s} hopping may stem from the following virtual hopping processes: One electron first hops from the p_x to the d_{xz} , and then, an electron in the p_y at the same As(Se) site can hop to the p_x . Finally, an electron in the d_{yz} orbital hops to the p_y . In such a process, the reflection symmetry is broken due to the existence of the hopping between the p_x and p_y orbitals at the same As(Se) site when the two orbitals host a total of 3 electrons, which is possible if the on-site Hubbard interaction U in p orbitals is sufficiently large such that the degeneracy of p_x and p_y is broken, a result of the standard Jahn–Teller effect.

F. The coupling between two S_4 isospins and S_4 symmetry breaking

The couplings between the two isospins can either keep the S_4 symmetry or break it. Without breaking the translational symmetry, the coupling between two orbitals can be written as

$$\hat{H}_c = \sum_{k,\alpha} f_\alpha(k) \hat{G}_\alpha(k) + \sum_{k,\bar{\alpha}} f_{\bar{\alpha}}(k) \hat{G}_{\bar{\alpha}}(k), \quad (13)$$

where $\hat{G}_\alpha(k)$ and $\hat{G}_{\bar{\alpha}}(k)$ are operators constructed according to the S_4 one-dimensional representations, as follows:

$$\hat{G}_1(k) = \sum_\sigma c_{k\sigma}^+ \hat{d}_{k\sigma} + c_{k+Q\sigma}^+ \hat{d}_{k+Q\sigma} + \text{H.c.}, \quad (14)$$

$$\hat{G}_2(k) = \sum_\sigma c_{k\sigma}^+ \hat{d}_{k\sigma} - c_{k+Q\sigma}^+ \hat{d}_{k+Q\sigma} + \text{H.c.}, \quad (15)$$

$$\hat{G}_3(k) = \sum_\sigma c_{k\sigma}^+ \hat{d}_{k+Q\sigma} + c_{k+Q\sigma}^+ \hat{d}_{k\sigma} + \text{H.c.}, \quad (16)$$

$$\hat{G}_4(k) = \sum_\sigma c_{k\sigma}^+ \hat{d}_{k+Q\sigma} - c_{k+Q\sigma}^+ \hat{d}_{k\sigma} + \text{H.c.}, \quad (17)$$

$$\hat{G}_{\bar{1}}(k) = \sum_\sigma i(c_{k\sigma}^+ \hat{d}_{k\sigma} + c_{k+Q\sigma}^+ \hat{d}_{k+Q\sigma} - \text{H.c.}), \quad (18)$$

$$\hat{G}_{\bar{2}}(k) = \sum_\sigma i(c_{k\sigma}^+ \hat{d}_{k\sigma} - c_{k+Q\sigma}^+ \hat{d}_{k+Q\sigma} - \text{H.c.}), \quad (19)$$

$$\hat{G}_{\bar{3}}(k) = \sum_\sigma i(c_{k\sigma}^+ \hat{d}_{k+Q\sigma} + c_{k+Q\sigma}^+ \hat{d}_{k\sigma} - \text{H.c.}), \quad (20)$$

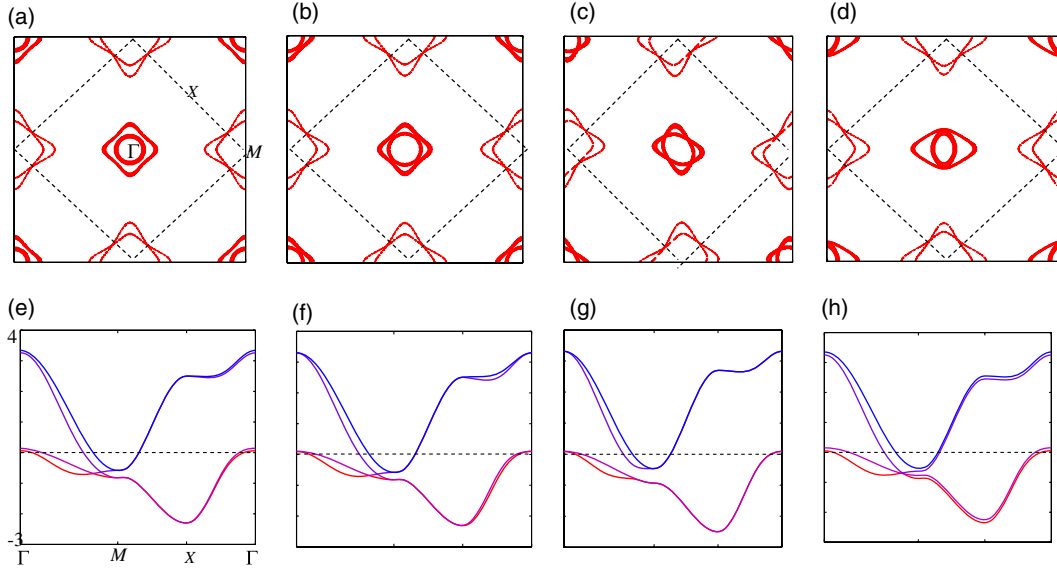


FIG. 6. Fermi surfaces and band dispersions in the presence of the S_4 symmetry breaking: (a),(e) $t_{b1} = 0.005$ in Eq. (22); (b),(f) $t_{bt} = 0.05$ in Eq. (23); (c),(g) $t_{bo} = 0.05$ in Eq. (24); (d),(h) $t_{bso} = 0.05$ in Eq. (25). Other parameters are the same as in Fig. 5. The y axis for (e)–(h) is in units of E(ev).

$$\hat{G}_{\bar{4}}(k) = \sum_{\sigma} i(c_{k\sigma}^+ \hat{d}_{k+Q\sigma} - c_{k+Q\sigma}^+ \hat{d}_{k\sigma} - \text{H.c.}). \quad (21)$$

We discuss a few examples that can cause the S_4 symmetry breaking:

$$\hat{H}_{b1} = \sum_k 2t_{b1}(\cos k_x + \cos k_y)(\hat{c}_{k\sigma}^+ \hat{d}_{k+Q\sigma} + \text{H.c.}), \quad (22)$$

$$\hat{H}_{bt} = \sum_k 4it_{bt} \sin k_x \sin k_y (\hat{c}_{k\sigma}^+ \hat{d}_{k+Q\sigma} - \text{H.c.}), \quad (23)$$

$$\hat{H}_{bo} = \sum_k t_{bo}(\hat{c}_{k\sigma}^+ \hat{c}_{k+Q\sigma} - d_{k\sigma}^+ \hat{d}_{k+Q\sigma}), \quad (24)$$

$$\hat{H}_{bso} = \sum_k t_{bso}(\hat{c}_{k\sigma}^+ \hat{c}_{k\sigma} - d_{k\sigma}^+ \hat{d}_{k\sigma}). \quad (25)$$

The t_{b1} term breaks the S_4 symmetry to lift the degeneracy at Γ point; t_{bt} breaks the time-reversal symmetry; t_{bo} indicates a ferro-orbital ordering; and t_{bso} indicates a staggered-orbital ordering. These terms can be generated either spontaneously or externally, and their effects can be explicitly observed in the change of the band structure and degeneracy lifting, as shown in Fig. 6, where the changes of band structures and Fermi surfaces due to the symmetry-breaking terms are plotted. It will be fascinating to study the interplay between the S_4 symmetry and other broken symmetries in this system.

IV. CLASSIFICATION OF THE SUPERCONDUCTING ORDERS ACCORDING TO THE S_4 SYMMETRY

The presence of the S_4 symmetry brings us to a new symmetry classification of the superconducting phases. The S_4 point group has four one-dimensional representations, including A , B , and $2E$. In the A state, the S_4 symmetry is maintained. In the B state, the state changes sign under the S_4 transformation. In the $2E$ state, the state obtains a $\pm\pi/2$ phase under the S_4 transformation. Therefore, the $2E$ state breaks the C_2 rotational symmetry as well as the time-reversal symmetry.

Since the S_4 transformation includes two parts, a 90° degree rotation and a reflection along the c axis, the S_4 -symmetry classification leads to a natural correlation between the rotation in the a - b plane and c -axis reflection symmetries in a SC phase. In the A phase, rotation and c -axis reflection symmetries can both be broken, while in the B phase, one, and only one, of them can be broken. This correlation, in principle, may be observed by applying external symmetry breaking. For example, even in the A phase where the rotational symmetry is not broken, we can force the c -axis phase-flip to obtain the phase change in the a - b plane.

As shown in this paper, the iron-based superconductors are rather unique with respect to the S_4 symmetry. These superconductors have two isospin components governed by the symmetry. This isospin degree of freedom and the interaction between the components could lead to many novel phases. Future study can explore these possibilities.

Here, we specifically discuss the S_4 -symmetry aspects in the proposed A_{1g} s -wave state, a most-likely phase if it is

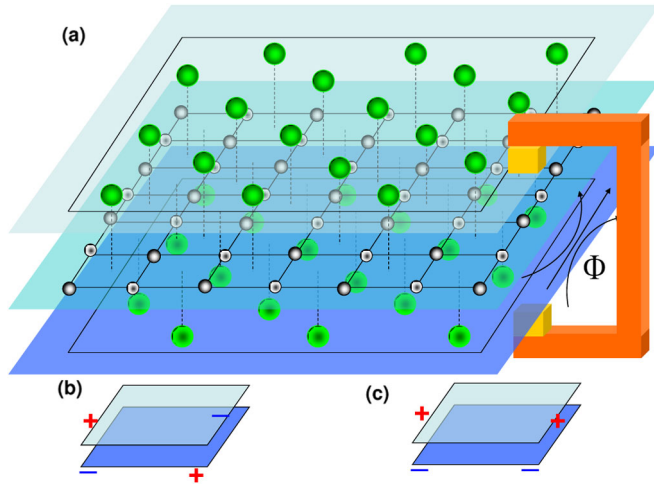


FIG. 7. (a) An illustration of a single Fe-As(Se) layer and the setup for a dc SQUIDS measurement to measure the sign change of the SC phase between top and bottom As(Se) layers. (b) The phase distribution in the A phase of the A_{1g} s -wave state in the view of a d -wave picture (red for one isospin component and blue for the other). (c) The phase distribution in the B phase of the A_{1g} s -wave state.

driven by the repulsive interaction or strong antiferromagnetism in iron-based superconductors [29] as we have shown earlier. First, let us clarify the terminology issues. The A_{1g} s -wave pairing symmetry is classified according to the D_{4h} point group. This classification is not correct in the view of the true lattice symmetry. However, for each isospin component, we can still use it. Here we treat it as a state where the superconducting order $\Delta \propto \cos k_x \cos k_y$ [29]. Since the A_{1g} phase is equivalent to the d wave in cuprates in a different gauge setting, the d -wave picture is more transparent regarding the sign change of the phase of the superconducting order parameter in the real space. As shown in Fig. 1, the sign of the SC order alternates between neighboring squares in the iron lattice.

Based on the underlying electronic structure revealed here with respect to the S_4 symmetry, the A_{1g} state can have two different phases: A and B . In the A phase,

$$\langle \hat{c}_{k\uparrow} \hat{c}_{-k\downarrow} \rangle = \langle \hat{d}_{k\uparrow} \hat{d}_{-k\downarrow} \rangle = \Delta_0 \cos k_x \cos k_y, \quad (26)$$

and in the B phase,

$$\langle \hat{c}_{k\uparrow} \hat{c}_{-k\downarrow} \rangle = -\langle \hat{d}_{k\uparrow} \hat{d}_{-k\downarrow} \rangle = \Delta_0 \cos k_x \cos k_y. \quad (27)$$

Therefore, in the view of the d -wave picture, in both A and B phases, the phase of the superconducting order parameter for each component alternates between neighboring squares. The alternation corresponds to the sign change between the top and bottom planes in view of the S_4 symmetry. However, in the A phase, since the S_4 symmetry is not violated, the relative phase between the two components is equal to π in space, while, in the B phase, the relative phase is zero. A picture of the phase distribution of the two isospin

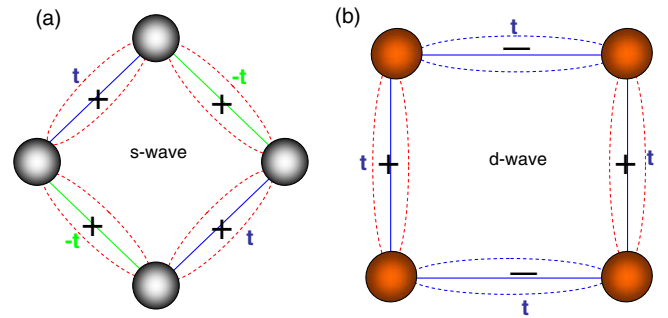


FIG. 8. A sketch of the correlation between the hopping and pairing symmetries for both iron-based superconductors and cuprates. The black (a) and the bronze (b) balls represent Fe and Cu atoms, respectively. The blue and green solid lines indicate that the hoppings between two connected atoms have opposite signs. The red and blue dashed lines indicate that the SC pairings between two connected atoms have opposite signs.

components in the A and B phases is illustrated in Figs. 7(b) and 7(c).

The sign change of the order parameter or the phase shift of π between the top and bottom planes along the c axis can be detected by standard magnetic-flux modulation of dc superconducting quantum interference devices (SQUIDS) measurements [36]. If we consider a single Fe-As(Se) trilayer structure, which has recently been successfully grown by the molecular-beam epitaxy technique [11,12], we can design a standard dc SQUIDS as shown in Fig. 7(a) following the similar experimental setup to determine the d -wave pairing in cuprates described in Ref. [36]. For the B phase, there is no question that the design can repeat the previous results in cuprates. However, if the tunneling matrix elements for two components are not symmetric, even in the A phase, this design can obtain the signal of the π phase shift, since the two components are weakly coupled and each of them has a π phase shift. For the B phase, the phase shift may be preserved even in bulk materials [55]. However, for the A phase, it will be difficult to detect the phase shift in bulk materials. A more clever design is needed. Measuring the phase shift between the upper and lower As(Se) planes will be a smoking-gun experiment to verify the model and determine that iron-based superconductors and cuprates share an identical superconducting mechanism.

V. DISCUSSION AND SUMMARY

We have shown that the A_{1g} s -wave pairing in iron-based superconductors is a d -wave pairing when viewed in a different gauge setting. This equivalence answers an essential question: Why can a A_{1g} s -wave pairing be robust regardless of the presence or absence of the hole pockets? With repulsive interactions, a sign-changed order parameter in a superconducting state is usually inevitable. This statement is only true, however, when the hopping parameters follow the same lattice symmetry. Gauge

TABLE I. A list of the close connections between iron-based superconductors (iron SCs) and cuprates.

Properties	Iron superconductors	Cuprates
Pairing symmetry	s wave	d wave
Underlying hopping symmetry	d wave	s wave
Dominant pairing form	$\cos k_x \cos k_y$	$\cos k_x - \cos k_y$
Pairing-classification symmetry	S_4	C_4
AF coupling	NNN J_2	NN J_1
Sign change in real space	c axis	a - b plane
Filling density	half filling	half filling

transformation can exchange the phases between superconducting order parameters and hopping parameters. In the case of cuprates, the d -wave order parameter can be transformed to an s -wave form by changing hopping parameters to obey d -wave symmetry. As we pointed out earlier, the NNN hopping in our model is close to a d -wave symmetry, rather than an s -wave symmetry. This is the essential reason why the superconducting order can have an s -wave form and still be stable in iron-based superconductors. A simple picture of this discussion is illustrated in Fig. 8. The vanishing of the hole pockets in electron-overdoped iron-chalcogenides indicates that the hopping is even more d -wave-like in these materials. This case supports stronger s -wave pairing, which has indeed been observed recently [12,13]. The presence of the dominant form $\cos k_x \cos k_y$ is also directly linked to the d -wave pairing form ($\cos k'_x - \cos k'_y$) because of the stable AF J_2 coupling, similar to cuprates [56]. Moreover, since the different gauge setting does not alter physical measurements, a phase-sensitive measurement should reveal a π phase shift in the real space along the c axis for each component in the A_{1g} s -wave state, just like the phase shift along the a and b directions in the d -wave pairing state of cuprates.

We can now ask the question of how the physics in the cuprates and in the iron-based superconductors are related to each other. In Table. I, we list the close relationships between two high- T_c superconductors. From the table, it is clear that determining the physical properties of iron-based superconductors listed in the table can help to determine the high- T_c superconducting mechanism.

The microscopic model we have put forward completely changes the view of the origin of the generation of sign-changed s^\pm pairing symmetry in iron-pnictides. Many theories argued before that the origin is the scattering between electron pockets at M and hole pockets at Γ due to repulsive interactions [6,9]. Within the framework proposed by our model, the analysis of the sign change should be examined after taking the gauge transformation so that the underlying hopping parameters become symmetric. In this case, the sign change is driven by scatterings between all pockets, including both hole and electron pockets, located at two d -wave antinodal X' points.

Therefore, the scattering between electron pockets is also important.

While the model appears to be rotationally invariant due to the S_4 symmetry, the dynamics of each isospin component is intrinsically nematic. A small S_4 symmetry breaking can easily lead to an overall electronic nematic state. The electronic nematic state has been observed by many experimental techniques [57] and studied by different theoretical models [58–65]. The underlying electronic structure in the model can provide a straightforward microscopic understanding of the interplay of all different degree of freedoms based on the S_4 symmetry breaking.

It is worth point out that in our model, if t_{1s} is generated by a mixing of different orbital characters, it is generally not limited to the NN hopping. It can be a function of k that satisfies $t_{1s}(k) = -t_{1s}(k + Q)$ so that it breaks σ_v symmetry. The value of t_c may be not small. However, both t_{1s} and t_c have very limited effects on the electron pockets. While we may use a different set of t_{1s} and t_c to fit the electronic structure, the key physics in the paper remains the same because the essential physics stems from the NNN hoppings.

In summary, we have shown that the underlying electronic structure responsible for superconductivity at low energy in iron-based superconductors, is essentially two nearly degenerate electronic structures governed by the S_4 symmetry. We have demonstrated that the s -wave pairing in iron-based superconductors is equivalent to the d -wave in cuprates. A similar conclusion has also been reached in the study of a two-layer Hubbard model[66]. The S_4 -symmetry model reveals possible new superconducting states and suggests that the phase shift in the SC state in real space is along the c axis. These results strongly support the assertion that the microscopic superconducting mechanism for cuprates and iron-based superconductors (including both iron pnictides and iron chalcogenides) is identical. Our model establishes a new foundation for understanding and exploring properties of iron-based superconductors, a unique, elegant, and beautiful class of superconductors.

ACKNOWLEDGMENTS

J.H. thanks H. Ding, D.L. Feng, S.A. Kivelson, P. Coleman, X. Dai, Y.P. Wang, E. A. Kim, and F. Wang for useful discussions. J.H. especially thanks H. Ding, F. Wang, M. Fischer, and W. Li for the discussion of the symmetry properties of the model. This work is supported by the Ministry of Science and Technology of China 973 program 2012CB821400 and the National Science Foundation of China Grant No. NSFC-1190024.

- [1] Y. Kamihara, T. Watanabe, M. Hirano, and H. Hosono, *Iron-Based Layered Superconductor*

- La[O_{1-x}F_x]FeAs ($x = 0.05-0.12$) with $T_c = 26$ K, *J. Am. Chem. Soc.* **130**, 3296 (2008).
- [2] X. H. Chen, T. Wu, G. Wu, R. H. Liu, H. Chen, and D. F. Fang, *Superconductivity at 43 K in SmFeAsO_{1-x}F_x*, *Nature (London)* **453**, 761 (2008).
- [3] G. F. Chen, Z. Li, D. Wu, G. Li, W. Z. Hu, J. Dong, P. Zheng, J. L. Luo, and N. L. Wang, *Superconductivity at 41 K and Its Competition with Spin-Density-Wave Instability in Layered CeO_{1-x}F_xFeAs*, *Phys. Rev. Lett.* **100**, 247002 (2008).
- [4] Jiangang Guo, Shifeng Jin, Gang Wang, Shunchong Wang, Kaixing Zhu, Tingting Zhou, Meng He, and Xiaolong Chen, *Superconductivity in the Iron Selenide K_xFe₂Se₂ ($0 \leq x \leq 1.0$)*, *Phys. Rev. B* **82**, 180520(R) (2010).
- [5] P. J. Hirschfeld, M. M. Korshunov, and I. I. Mazin, *Gap Symmetry and Structure of Fe-based Superconductors*, arXiv:1106.3712.
- [6] David Johnston, *The Puzzle of High Temperature Superconductivity in Layered Iron Pnictides and Chalcogenides*, *Adv. Phys.* **59**, 803 (2010).
- [7] S. Raghu, Xiao-Liang Qi, Chao-Xing Liu, D. J. Scalapino, and Shou-Cheng Zhang, *Minimal Two-Band Model of the Superconducting Iron Oxyprictides*, *Phys. Rev. B* **77**, 220503 (2008).
- [8] Patrick A. Lee and Xiao-Gang Wen, *Spin-Triplet p-Wave Pairing in a Three-Orbital Model for Iron Pnictide Superconductors*, *Phys. Rev. B* **78**, 144517 (2008).
- [9] I. I. Mazin, D. J. Singh, M. D. Johannes, and M. H. Du, *Unconventional Superconductivity with a Sign Reversal in the Order Parameter of LaFeAsO_{1-x}F_x*, *Phys. Rev. Lett.* **101**, 057003 (2008).
- [10] Kazuhiko Kuroki, Seiichiro Onari, Ryotaro Arita, Hidetomo Usui, Yukio Tanaka, Hiroshi Kontani, and Hideo Aoki, *Unconventional Pairing Originating from the Disconnected Fermi Surfaces of Superconducting LaFeAsO_{1-x}F_x*, *Phys. Rev. Lett.* **101**, 087004 (2008).
- [11] D. Liu, W. Zhang, D. Mou, J. He, Y.-B. Ou, Q.-Y. Wang, Z. Li, L. Wang, L. Zhao, S. He *et al.*, *Electronic Origin of High Temperature Superconductivity in Single-Layer FeSe Superconductor*, arXiv:1202.5849.
- [12] Q.-Y. Wang, Z. Li, W.-H. Zhang, Z.-C. Zhang, J.-S. Zhang, W. Li, H. Ding, Y.-B. Ou, P. Deng, K. Chang *et al.*, *Interface Induced High Temperature Superconductivity in Single Unit-Cell FeSe Films on SrTiO₃*, arXiv:1201.5694.
- [13] L. Sun, X.-J. Chen, J. Guo, P. Gao, Q.-Z. Huang, H. Wang, M. Fang, X. Chen, G. Chen, Q. Wu *et al.*, *Re-emerging Superconductivity at 48 Kelvin in Iron Chalcogenides*, *Nature (London)* **483**, 67 (2012).
- [14] H. Ding, P. Richard, K. Nakayama, K. Sugawara, T. Arakane, Y. Sekiba, A. Takayama, S. Souma, T. Sato, T. Takahashi *et al.*, *Observation of Fermi-Surface-Dependent Nodeless Superconducting Gaps in Ba_{0.6}K_{0.4}Fe₂As₂*, *Europhys. Lett.* **83**, 47001 (2008).
- [15] Zhao Lin, Liu Hai-Yun, Zhang Wen-Tao, Meng Jian-Qiao, Jia Xiao-Wen, Liu Guo-Dong, Dong Xiao-Li, Chen Gen-Fu, Luo Jian-Lin, Wang Nan-Lin *et al.*, *Multiple Nodeless Superconducting Gaps in (Ba_{0.6}K_{0.4})Fe₂As₂ Superconductor from Angle-Resolved Photoemission Spectroscopy Superconductor*, *Chin. Phys. Lett.* **25**, 4402 (2008).
- [16] Y. Zhang, L. X. Yang, F. Chen, B. Zhou, X. F. Wang, X. H. Chen, M. Arita, K. Shimada, H. Namatame, M. Taniguchi, J. P. Hu, B. P. Xie, and D. L. Feng, *Out-of-Plane Momentum and Symmetry-Dependent Energy Gap of the Pnictide Ba_{0.6}K_{0.4}Fe₂As₂ Superconductor Revealed by Angle-Resolved Photoemission Spectroscopy*, *Phys. Rev. Lett.* **105**, 117003 (2010).
- [17] X.-P. Wang, T. Qian, P. Richard, P. Zhang, J. Dong, H.-D. Wang, C.-H. Dong, M.-H. Fang, and H. Ding, *Strong Nodeless Pairing on Separate Electron Fermi Surface Sheets in (Tl, K)Fe₂Se₂ Probed by ARPES*, *Europhys. Lett.* **93**, 57001 (2011).
- [18] Y. Zhang, L. X. Yang, M. Xu, Z. R. Ye, F. Chen, C. He, H. C. Xu, J. Jiang, B. P. Xie, J. J. Ying *et al.*, *Nodeless Superconducting Gap in A_xFe₂Se₂ (A = K, Cs) Revealed by Angle-Resolved Photoemission Spectroscopy*, *Nature Mater.* **10**, 273 (2011).
- [19] Daixiang Mou, Shanyu Liu, Xiaowen Jia, Junfeng He, Yingying Peng, Lin Zhao, Li Yu, Guodong Liu, Shaolong He, Xiaoli Dong *et al.*, *Distinct Fermi Surface Topology and Nodeless Superconducting Gap in a (Tl_{0.58}Rb_{0.42})Fe_{1.72}Se₂ Superconductor*, *Phys. Rev. Lett.* **106**, 107001 (2011).
- [20] K. Nakayama, T. Takahashi, P. Richard, T. Sato and H. Ding, *Fe-Based Superconductors: An Angle-Resolved Photoemission Spectroscopy Perspective*, *Rep. Prog. Phys.* **74**, 124512 (2011).
- [21] K. Nakayama, T. Sato, P. Richard, Y.-M. Xu, Y. Sekiba, S. Souma, G. F. Chen, J. L. Luo, N. L. Wang, H. Ding, and T. Takahashi, *Superconducting Gap Symmetry of Ba_{0.6}K_{0.4}Fe₂As₂ Studied by Angle-Resolved Photoemission Spectroscopy*, *Europhys. Lett.* **85**, 67002 (2009).
- [22] K. Umezawa, Y. Li, H. Miao, K. Nakayama, Z.-H. Liu, P. Richard, T. Sato, J. B. He, D.-M. Wang, G. F. Chen *et al.*, *Unconventional Anisotropic s-Wave Superconducting Gaps of the LiFeAs Iron-Pnictide Superconductor*, *Phys. Rev. Lett.* **108**, 037002 (2012).
- [23] Z.-H. Liu, P. Richard, K. Nakayama, G.-F. Chen, S. Dong, J.-B. He, D.-M. Wang, T.-L. Xia, K. Umezawa, T. Kawahara *et al.*, *Unconventional Superconducting Gap in NaFe_{0.95}Co_{0.05}As Observed by Angle-Resolved Photoemission Spectroscopy*, *Phys. Rev. B* **84**, 064519 (2011).
- [24] Fa Wang, Hui Zhai, Ying Ran, Ashvin Vishwanath, and Dung-Hai Lee, *Functional Renormalization-Group Study of the Pairing Symmetry and Pairing Mechanism of the FeAs-Based High-Temperature Superconductor*, *Phys. Rev. Lett.* **102**, 047005 (2009).
- [25] R. Thomale, C. Platt, J. P. Hu, C. Honerkamp, and B. A. Bernevig, *Functional Renormalization-Group Study of the Doping Dependence of Pairing Symmetry in the Iron Pnictide Superconductors*, *Phys. Rev. B* **80**, 180505(R) (2009).
- [26] Ronny Thomale, Christian Platt, Werner Hanke, Jiangping Hu, and B. Andrei Bernevig, *Exotic d-Wave Superconducting State of Strongly Hole-Doped K_xBa_{1-x}Fe₂As₂*, *Phys. Rev. Lett.* **107**, 117001 (2011).
- [27] A. V. Chubukov, D. V. Efremov, and I. Eremin, *Magnetism, Superconductivity, and Pairing Symmetry in*

- Iron-Based Superconductors*, *Phys. Rev. B* **78**, 134512 (2008).
- [28] Vladimir Cvetkovic and Zlatko Tesanovic, *Valley Density-Wave and Multiband Superconductivity in Iron-Based Pnictide Superconductors*, *Phys. Rev. B* **80**, 024512 (2009).
- [29] K. J. Seo, B. A. Bernevig, and J. P. Hu, *Pairing Symmetry in a Two-Orbital Exchange Coupling Model of Oxypnictides*, *Phys. Rev. Lett.* **101**, 206404 (2008).
- [30] Chen Fang, Yang-Le Wu, Ronny Thomale, B. Andrei Bernevig, and Jiangping Hu, *Robustness of s -Wave Pairing in Electron-Overdoped $A_{1-y}Fe_{2-x}Se_2$ ($A = K, Cs$)*, *Phys. Rev. X* **1**, 011009 (2011).
- [31] Qimiao Si and Elihu Abrahams, *Strong Correlations and Magnetic Frustration in the High T_c Iron Pnictides*, *Phys. Rev. Lett.* **101**, 076401 (2008).
- [32] Jiangping Hu and Hong Ding, *Local Antiferromagnetic Exchange and Collaborative Fermi Surface as Key Ingredients of High Temperature Superconductors*, *Sci. Rep.* **2**, 381 (2012) [<http://www.ncbi.nlm.nih.gov/pubmed/22536479>].
- [33] Jiangping Hu, Bao Xu, Wuming Liu, Ning-ning Hao, and Yupeng Wang, *Unified Minimum Effective Model of Magnetic Properties of Iron-Based Superconductors*, *Phys. Rev. B* **85**, 144403 (2012).
- [34] Xiaoli Lu, Chen Fang, Wei-Feng Tsai, Yongjin Jiang, and Jiangping Hu, *s -Wave Superconductivity with Orbital-Dependent Sign Change in Checkerboard Models of Iron-Based Superconductors*, *Phys. Rev. B* **85**, 054505 (2012).
- [35] E. Berg, S. A. Kivelson, and D. J. Scalapino, *Properties of a Diagonal Two-Orbital Ladder Model of the Iron Pnictide Superconductors*, *Phys. Rev. B* **81**, 172504 (2010).
- [36] D. A. Wollman, D. J. Van Harlingen, W. C. Lee, D. M. Ginsberg, and A. J. Leggett, *Experimental Determination of the Superconducting Pairing State in YBCO from the Phase Coherence of YBCO-Pb dc SQUIDS*, *Phys. Rev. Lett.* **71**, 2134 (1993).
- [37] D. J. Van Harlingen, *Phase-Sensitive Tests of the Symmetry of the Pairing State in the High-Temperature Superconductors—Evidence for $d_{x^2-y^2}$ Symmetry*, *Rev. Mod. Phys.* **67**, 515 (1995).
- [38] C. C. Tsuei and J. R. Kirtley, *Pairing Symmetry in Cuprate Superconductors*, *Rev. Mod. Phys.* **72**, 969 (2000).
- [39] E. Berg, S. A. Kivelson, and D. J. Scalapino, *A Twisted Ladder: Relating the Fe Superconductors to the High- T_c Cuprates*, *New J. Phys.* **11**, 085007 (2009).
- [40] D. J. Scalapino, *Condensed Matter Physics: The Cuprate Pairing Mechanism*, *Science* **284**, 1282 (1999).
- [41] J. P. Hu, N. Hao, and H. Ding (to be published).
- [42] L. X. Yang, B. P. Xie, Y. Zhang, C. He, Q. Q. Ge, X. F. Wang, X. H. Chen, M. Arita, J. Jiang, K. Shimada *et al.*, *Surface and Bulk Electronic Structures of LaFeAsO Studied by Angle-Resolved Photoemission Spectroscopy*, *Phys. Rev. B* **82**, 104519 (2010).
- [43] D. H. Lu, M. Yi, S.-K. Mo, J. G. Analytis, J.-H. Chu, A. S. Erickson, D. J. Singh, Z. Hussain, T. H. Geballe, I. R. Fisher, and Z.-X. Shen, *ARPES Studies of the Electronic Structure of LaOFe(P, As)*, *Physica (Amsterdam)* **469C**, 452 (2009).
- [44] Fei Chen, Bo Zhou, Yan Zhang, Jia Wei, Hong-Wei Ou, Jia-Feng Zhao, Cheng He, Qing-Qin Ge, Masashi Arita, Kenya Shimada *et al.*, *Electronic Structure of $Fe_{1.04}Te_{0.66}Se_{0.34}$* , *Phys. Rev. B* **81**, 014526 (2010).
- [45] O. J. Lipscombe, G. F. Chen, Chen Fang, T. G. Perring, D. L. Abernathy, A. D. Christianson, Takeshi Egami, Nanlin Wang, Jiangping Hu, and Pengcheng Dai, *Spin Waves in the Magnetically Ordered Iron Chalcogenide $Fe_{1.05}Te$* , *Phys. Rev. Lett.* **106**, 057004 (2011).
- [46] Miaoyin Wang, Chen Fang, Dao-Xin Yao, GuoTai Tan, Leland W. Harriger, Yu Song, Tucker Netherton, Chenglin Zhang, Meng Wang, Matthew B. Stone *et al.*, *Spin Waves and Magnetic Exchange Interactions in Insulating $Rb_{0.89}Fe_{1.58}Se_2$* , *Nature Commun.* **2**, 580 (2011).
- [47] P. W. Anderson, P. A. Lee, M. Randeria, T. M. Rice, N. Trivedi, and F. C. Zhang, *The Physics behind High-Temperature Superconducting Cuprates: The “Plain Vanilla” Version of RVB*, *J. Phys. Condens. Matter* **16**, R755 (2004).
- [48] P. A. Lee, N. Nagaosa, and X.-G. Wen, *Doping a Mott Insulator: Physics of High-Temperature Superconductivity*, *Rev. Mod. Phys.* **78**, 17 (2006).
- [49] J. Zhao, D. T. Adroja, D.-X. Yao, R. Bewley, S. L. Li, X. F. Wang, G. Wu, X. H. Chen, J. P. Hu, and P. C. Dai, *Spin Waves and Magnetic Exchange Interactions in $CaFe_2As_2$* , *Nature Phys.* **5**, 555 (2009).
- [50] J. Hu (to be published).
- [51] Y. Zhang, F. Chen, C. He, B. Zhou, B. P. Xie, C. Fang, W. F. Tsai, X. H. Chen, H. Hayashi, J. Jiang *et al.*, *Orbital Characters of Bands in the Iron-Based Superconductor $BaFe_{1.85}Co_{0.15}As_2$* , *Phys. Rev. B* **83**, 054510 (2011).
- [52] Fei Chen, Bo Zhou, Yan Zhang, Jia Wei, Hong-Wei Ou, Jia-Feng Zhao, Cheng He, Qing-Qin Ge, Masashi Arita, Kenya Shimada *et al.*, *Electronic Structure of $Fe_{1.04}Te_{0.66}Se_{0.34}$* , *Phys. Rev. B* **81**, 014526 (2010).
- [53] Z.-H. Liu, P. Richard, N. Xu, G. Xu, Y. Li, X.-C. Fang, L.-L. Jia, G.-F. Chen, D.-M. Wang, J.-B. He, *et al.*, *Three-Dimensionality and Orbital Characters of Fermi Surface in $(Tl, Rb)_yFe_{2-x}Se_2$* , [arXiv:1202.6417v2](https://arxiv.org/abs/1202.6417v2).
- [54] M. F. Jensen, V. Brouet, E. Papalazarou, A. Nicolaou, A. Taleb-Ibrahimi, P. Le Fèvre, F. Bertran, A. Forget, and D. Colson, *Angle-Resolved Photoemission Study of the Role of Nesting and Orbital Orderings in the Antiferromagnetic Phase of $BaFe_2As_2$* , *Phys. Rev. B* **84**, 014509 (2011).
- [55] The 122 structure doubles the unit cell along the c axis. If it is in the B phase, it requires an odd number of iron layers to measure the sign change. We will discuss this issue in a future publication.
- [56] G. Kotliar and J. L. Liu, *Superexchange Mechanism and d -Wave Superconductivity*, *Phys. Rev. B* **38**, 5142 (1988).
- [57] I. R. Fisher, L. Degiorgi, and Z. X. Shen, *In-Plane Electronic Anisotropy of Underdoped “122” Fe-Arsenide Superconductors Revealed by Measurements of Detwinned Single Crystals*, *Rep. Prog. Phys.* **74**, 124506 (2011).
- [58] C. Fang, H. Yao, W. F. Tsai, J. P. Hu, and S. A. Kivelson, *Theory of Electron Nematic Order in LaFeAsO*, *Phys. Rev. B* **77**, 224509 (2008).
- [59] Cenke Xu, Markus Müller, and Subir Sachdev, *Ising and Spin Orders in the Iron-Based Superconductors*, *Phys. Rev. B* **78**, 020501(R) (2008).

- [60] Cenke Xu and Jiangping Hu, *Nematic Orders in Iron-Based Superconductors*, [arXiv:1112.2713](https://arxiv.org/abs/1112.2713).
- [61] I. I. Mazin and M. D. Johannes, *A Key Role for Unusual Spin Dynamics in Ferropnictides*, *Nature Phys.* **5**, 141 (2008).
- [62] F. Kruger, S. Kumar, J. Zaanen, and J. van den Brink, *Spin-Orbital Frustrations and Anomalous Metallic State in Iron-Pnictide Superconductors*, *Phys. Rev. B* **79**, 054504 (2009).
- [63] Weicheng Lv, Jiansheng Wu, and Philip Phillips, *Orbital Ordering Induces Structural Phase Transition and the Resistivity Anomaly in Iron Pnictides*, *Phys. Rev. B* **80**, 224506 (2009).
- [64] C.-C. Lee, W.-G. Yin, and W. Ku, *Ferro-orbital Order and Strong Magnetic Anisotropy in the Parent Compounds of Iron-Pnictide Superconductors*, *Phys. Rev. Lett.* **103**, 267001 (2009).
- [65] R.M. Fernandes, E. Abrahams, and J. Schmalian, *Anisotropic In-Plane Resistivity in the Nematic Phase of the Iron Pnictides*, *Phys. Rev. Lett.* **107**, 217002 (2011).
- [66] T.A. Maier and D.J. Scalapino, *Pair Structure and the Pairing Interaction in a Bilayer Hubbard Model for Unconventional Superconductivity*, *Phys. Rev. B* **84**, 180513(R) (2011).